J Therm Spray Tech (2018) 27:857–869
https://doi.org/10.1007/s11666-018-0725-z

PEER REVIEWED

Roles of Particle Size Distribution in Bimodal Feedstocks on the Deposition Behavior and Film Properties in Vacuum Kinetic Spraying

Hansol Kwon[1] · Hyungkwon Park[2] · Changhee Lee[1]

Submitted: 4 February 2018 / in revised form: 12 April 2018 / Published online: 7 June 2018

Abstract Vacuum kinetic spray (VKS), also called aerosol deposition method, is a spray process that makes it possible to fabricate dense ceramic films at room temperature. Although the deposition rate of VKS is better than conventional ceramic coating processes, the deposition properties are still poor for industrial use. In this respect, this work investigates the role of particle size on the deposition behavior by blending two alumina powders having different sizes. It results in suggestions for increasing the deposition efficiency and rate. The microstructure and mechanical properties of films revealed that nanosized particles directly took part in deposition and participated in increasing the deposition rate despite the low adhesion between crystallites. In contrast, relatively large submicron-sized particles mainly contributed to the coating consolidation via severe friction, which strengthened the fragment bonding. Submicron-sized particles also were indirectly deposited as crystallites after sufficient fragmentation. Therefore, it is suggested that the deposition behavior and film properties in VKS can be controlled by adjusting the mixing ratio of two alumina powders with different particle size ranges.

Keywords bimodal powder · particle size · thick ceramic film · vacuum kinetic spraying (VKS) process

✉ Changhee Lee
chlee@hanyang.ac.kr

[1] Kinetic Spray Coating Laboratory (NRL), Division of Materials Science and Engineering, Hanyang University, Seongdong-gu, Seoul 04763, South Korea

[2] Steel Application Engineering Team, Hyundai Steel Company, Dangjin-Si, Chungnam 31719, South Korea

Introduction

The vacuum kinetic spray (VKS) process, which is also referred to aerosol deposition method (ADM), has been highly regarded as a ceramic film technology. By using this process, it is possible to make a thin or thick ceramic film even at room temperature without any binder. Usually, dense ceramic film can be deposited on various types of substrate (metal, ceramic, and polymer) and various ceramic materials can be selected as a feedstock powder. In addition, the film growth rate is relatively high compared to conventional ceramic thin-film fabrication techniques. Because of these advantages, various researches have been performed for many applications (Ref 1-3).

Unfortunately, this process has been unacceptable to industrial field due to the low deposition efficiency which was reported to be around 0.1% (Ref 4). Also, when compared to a similar particle spray deposition processes, like thermal or kinetic spray (of cold spray), the deposition rate of VKS of 1-3 μm/min is still very insufficient. Due to these limitations of deposition characteristics, utilization of the VKS process has been limited to fabrication of relatively thin films or sometimes patterns of less than several microns thin (Ref 2, 3). Therefore, if the poor process efficiency is overcome, this deposition technique to be further applied over a wide range of industrial fields will be possible, such as thick ceramic coating, thick 2D patterning, or 3D printing.

In the VKS process, ceramic powders of submicron size are used and the particles fly and impact with a high velocity of $\sim$ 600 m/s (Ref 5, 6). Unlike the kinetic spray, the preheat treatment of powder and process gas usually does not exist. Thus, the kinetic energy of the particles is the only source of the bonding. Many studies indicated that particles are deposited via plasticity and fragmentation.

Finally, a film of nanocrystallinity with a flattened shape microstructure is formed (Ref 7-9).

Like other spray-coating processes, the feedstock particle size is critical for successful deposition of dense ceramic film in VKS. Because it is well known that the process window of VKS for ceramic particles is quite narrow, to reveal the proper particle size range has been an issue. J. Akedo once selected a spherical α-Al_2O_3 ultrafine particle with average particle size around 50 nm as a feedstock material. The result indicated that the film had pressed-like structure and easily delaminated even by a low external stress (Ref 2). D. Lee et al. also used three different types of Al_2O_3 powders with average particle size of 0.5, 3.6, and 3.9 μm. They reported that the deposition rate was decreased and film roughness was increased, with increasing particle size (Ref 10, 11). J. Exner et al. performed a broad range of experiment using 14 types of different Al_2O_3 powders with different sizes. From their results, the particles with high deposition rate generally were hard to form the strongly bonded and uniform film (Ref 12). Recently, L. Wang et al. conducted the research that dealt with the two Al_2O_3 particles with size of 80 and 400 nm. They also mentioned that the deposition rate was higher in case of the smaller particle (Ref 13). Through the above-mentioned studies, one can expect that the several tens of nanosized particles are good candidates for achieving higher deposition efficiency. The authors, however, also insisted that the film manufactured by those particles usually had poor adhesion. Considering that the room-temperature impact consolidation (RTIC) is essential for good substrate–particle or particle–particle intimacy, it is expected that those particles cannot transfer sufficient impact energy to the particle itself and pre-deposited particles. On the other hand, it was revealed that when the submicron-sized particles were used as a feedstock powder, a dense film was fabricated and consolidation phenomena were observed on the surface. It is clear that the deposition behavior of particles with different sizes is quite different. In our point of view, powders used in VKS usually have some size distribution from nanometers to micrometers. Thus, in an actual situation, the complex deposition phenomena may coexist. Unfortunately, there has been no such research in VKS that dealt with the bimodal state of powders so far.

Based on this situation, we focused on the reason of deposition characteristics and film mechanical properties. Bimodal feedstock powders were manufactured by blending two different sized Al_2O_3 powders with various ratios. The roles of particle depending on their sizes are discussed, and the change of the deposition rate, efficiency, and film properties were analyzed. These results are crucial to understanding the particle deposition process and improving the deposition characteristics of VKS process.

Experimental Method

Material Preparation

In this research, two kinds of Al_2O_3 powders with significantly different sizes were selected. The first one was a nanosized primary particle (1015WW, Nanostructured and Amorphous Materials, Inc.), while the second one had a submicron size (AL-160SG3, Showa Denko), as shown in Fig. 1(a) and (b), respectively (for convenience, each powder is denoted as nano- and submicron Al_2O_3 in this study). Nano-Al_2O_3 is comprised of 90% α- and 10% γ-phases, whereas submicron Al_2O_3 is 100% α-phase. Figure 2(a) and (b) shows the primary and secondary particle size distributions of each powder, where the secondary size indicates the agglomerated size of the powder. The primary and secondary particle sizes were measured by using image analyzer software (Image-pro plus 4.5) and the particle size distribution (PSD, Malstersizer 3000, Malvern), respectively. Nano-Al_2O_3 had average primary and secondary sizes of 0.028 and 1.21 μm (D_{10} of 0.066 μm and D_{90} of 3.18 μm), respectively. On the other hand, the submicron powder had average primary and secondary sizes of 0.31 and 0.95 μm (D_{10} of 0.354 μm and D_{90} of 1.58 μm), respectively. It is indicated that both types of powders have agglomerated state. Especially, nano-Al_2O_3 had an extremely larger secondary size than the primary size due to severe agglomeration resulting from the high surface energy despite sufficiently drying them at 130 °C in a vacuum dryer for several hours prior to the deposition experiments. Because two powders have similar average secondary particle size, it can be assumed that the particle impact velocity of particles is also similar.

To investigate the deposition behavior according to blending ratio, the two Al_2O_3 powders were blended at a certain ratio. In the first trial, to observe the overall deposition behavior, submicron and nano-Al_2O_3 were blended at ratios of 0:100, 25:75, 50:50, 75:25, and 100:0. For convenience, each blended powder is denoted as N0, N25, N50, N75, and N100. Then, in the second trial, to optimize the powder mixture ratio for thick film fabrication considering the film mechanical properties, each powder was blended at ratios of 90:10 (N90), 95:5 (N95), and 100:0 (N100). The blending ratio and notations of all powders are summarized in Table 1. Additionally, soda lime glass with dimensions of 75 × 25 × 1 mm^3 was chosen as the substrate material. All substrates and coatings were cleaned by ultrasonication for 5 min in ethanol to remove

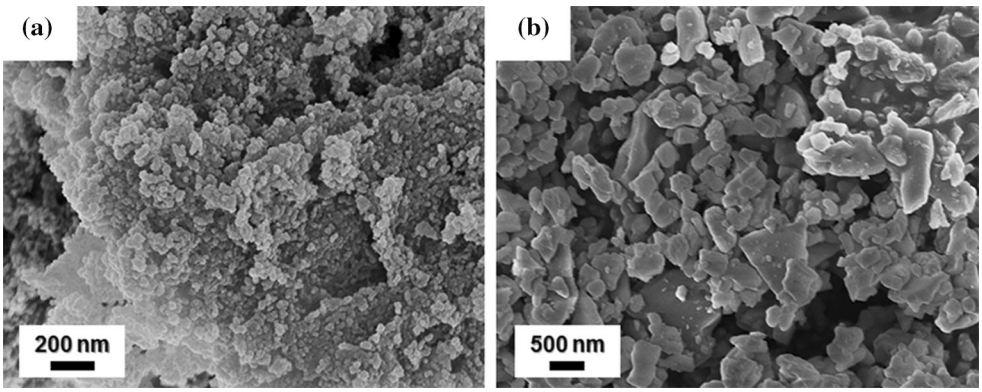

Fig. 1 FE-SEM micrographs of the powder morphologies: (a) nano- and (b) submicron Al_2O_3 powder

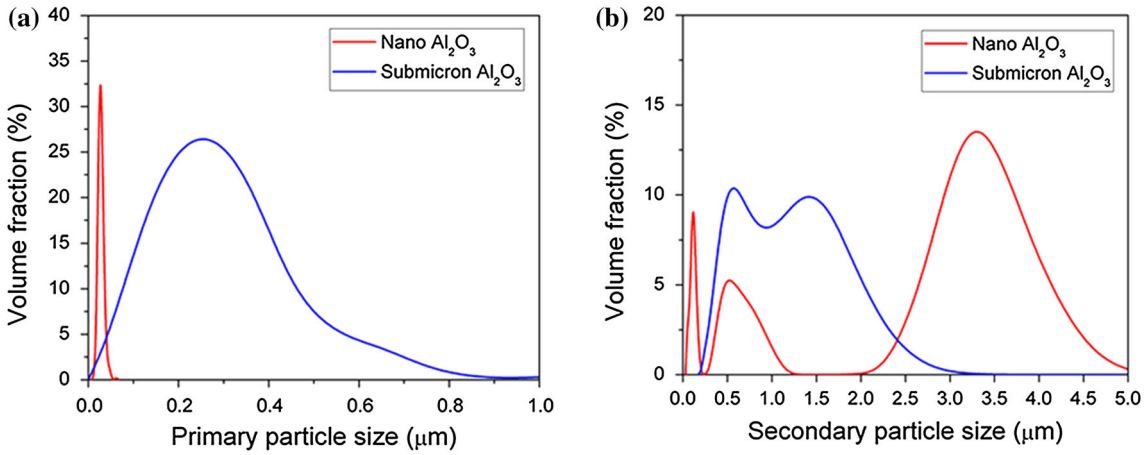

Fig. 2 (a) Primary and (b) secondary particle size distributions of nano- and submicron Al_2O_3 powders

Table 1 Blending ratios of the two powders

	First trials					Second trials	
Blended powder notation	N0	N25	N50	N75	N100	N90	N95
Submicron Al_2O_3, wt.%	0	25	50	75	100	90	95
Nano Al_2O_3, wt.%	100	75	50	25	0	10	5

contamination on the surface before and after the deposition experiments and totally dried.

Vacuum Kinetic Spraying Conditions

Each blended powder was deposited using the VKS process (Fig. 3). Firstly, each powder was input into an aerosol chamber, and then, it was aerosolized by chamber vibration. The deposition chamber was evacuated up to 6.0×10^{-2} Torr by rotary and booster pumps, after which helium gas, as the process gas, flowed and carried the aerosol particles to the deposition chamber. The particles were accelerated to around 600 m/s as measured in the previous report (Ref 5). Due to the difficulty of pressure control and nozzle change during the deposition experiments, the gas flow rate was adjusted to control the particle velocity in the VKS process (Ref 2, 5). In this study, the gas flow rate was set to 10 L/min to investigate the deposition behavior depending on the blending ratio. The following process variables are listed in Table 2. The deposition rate and efficiency of VKS were calculated by Eq 1 and 2. The substrate, as-coated sample and powder hopper weight were measured before and after VKS coating to calculate the coating and used powder weight using an electronic scale.

$$\text{Deposition rate } (\mu\text{m/min}) = \frac{\text{Average coating thickness } (\mu\text{m})}{\text{Total coating time (min)}} \quad \text{(Eq 1)}$$

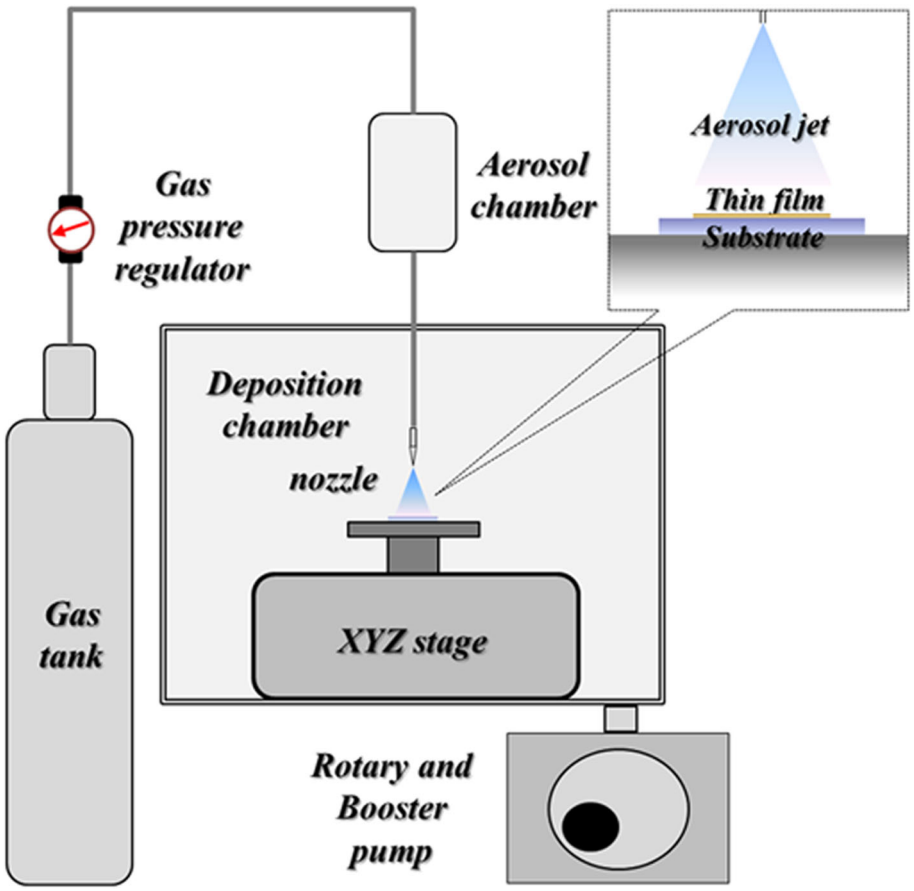

Fig. 3 Schematic image of the vacuum kinetic spraying system

Table 2 VKS parameters for the deposition of bimodal powders

Powder materials	Nano and submicron Al_2O_3
Substrate	Soda lime glass
Gas flow rate, L/min	10
Working distance, mm	10
Carrier gas	He
Gas pressure, MPa	0.6
Traverse speed, mm/s	1
Scan length, mm	20
Passes, #	10
Starting pressure, Torr	6.0×10^{-2}

$$\text{Deposition efficiency } (\%) = \frac{\text{Coating weight (g)}}{\text{Used powder weight (g)}} \times 100 \quad \text{(Eq 2)}$$

Characterization of the Powder and Coating

To observe the powder morphology, and cross-sectional microstructure of the coating, a field emission scanning electron microscope (FE-SEM, SIGMA, Carl Zeiss) was used. The coating profiles were measured by a surface profiler (Dektak XT, Bruker). The coating density was estimated by Eq 3 and 4. To measure the coating width and length, the image analysis software (Image-pro plus 4.5) was used.

$$\text{Coating density } \left(\text{g/cm}^3\right) = \frac{\text{Coating weight (g)}}{\text{Coating volume } (\text{cm}^3)} \quad \text{(Eq 3)}$$

$$\text{Coating volume } \left(\text{cm}^3\right) = \text{coating width} \times \text{length} \times \text{thickness} \quad \text{(Eq 4)}$$

The nanohardness and elastic modulus were assessed using a nanoindenter XP (MTS, Oak Ridge, TN) with a Berkovich tip. The indenter displacement was set to 500 nm, and the data were averaged over 10 measurements. In addition, a scratch tester (RB311 SKECH, RnB Co. Ltd.) was used to measure the adhesive bonding strength of each film according to ASTM C1624-05 (Ref 14). In the test, a Rockwell C-type diamond stylus with a conical shape indenter with an angle of 120° and a radius of 200 μm was used. The average value of 3 trials was considered as the adhesive strength. The detailed experimental

method can be readily found in our previous papers (Ref 15, 16).

Results and Discussion

Deposition Behavior Depending on Blending Ratio of the Two Powders

Figure 4(a) and (b) shows pictures of the deposits fabricated using the blended powders from N0 to N100 before and after ultrasonication, respectively. In Fig. 4(a), it is clearly observed that as the ratio of nano-Al_2O_3 increased, the particles were likely to be simply piled up, which is known as a pressed compact, but did not make a dense film (Ref 2). Although the form was heaped to several millimeters, it was easily peeled off even by a weak external stress such as ultrasonication, as observed in the N0, N25, and N50 samples in Fig. 4(b). In addition, because the simple deposited form was very porous and easily detached during the scratch test, the bonding strength could not be measured, and in this regard, it is difficult to be practically applied as a ceramic film. Thus, it is considered that there is a minimum percentage of submicron particles required to maintain sufficient adhesion. However, as the fraction of submicron Al_2O_3 increased, the deposited form became thin and dense with a change of color and transmittance. It is thought that the change is correlated with the impulse resulting from successive particle impacts, considering that the film was darkened as the particle velocity increased in VKS. In other words, the microstructure of the coating is gradually damaged by impacts with crystallite size reduction (boundary fraction increase), defects and lattice strain, amorphization, and non-equilibrium stoichiometry, which affects the transmittance and color (Ref 17). In this respect, it is considered that inflight submicron particles imparted a higher impulse than nanoparticles in spite of their similar high impact velocities (similar average size of secondary particles) (Ref 5).

To confirm the change of the microstructure, the cross sections of the N25, N50, and N75 specimens after unltrasonication were observed, as shown in Fig. 5. In Fig. 5(a)-(c), it is worth noting that a thick coating was formed even with only 10 passes. In the pictures, the coating thickness appears to increase as the submicron particle fraction increased. However, this is because the probability of delaminated regions is higher in case of high fraction of nano-Al_2O_3. When the nano-Al_2O_3 content was higher, the coating was easily peeled off during the sampling process. Especially, the loss of N25 and N50 coating was greater than N75 as also shown in Fig. 4. This means that as the quantity of nano-Al_2O_3 increases, a thick coating can be readily formed with low the bonding strength. On the other hand, it can be speculated that the quantity of submicron powder is related to the bonding strength considering delamination during ultrasonication in Fig. 4.

Figure 5(d)-(f) shows higher-magnification images of Fig. 5(a)-(c). In the figures, two points are worthy of

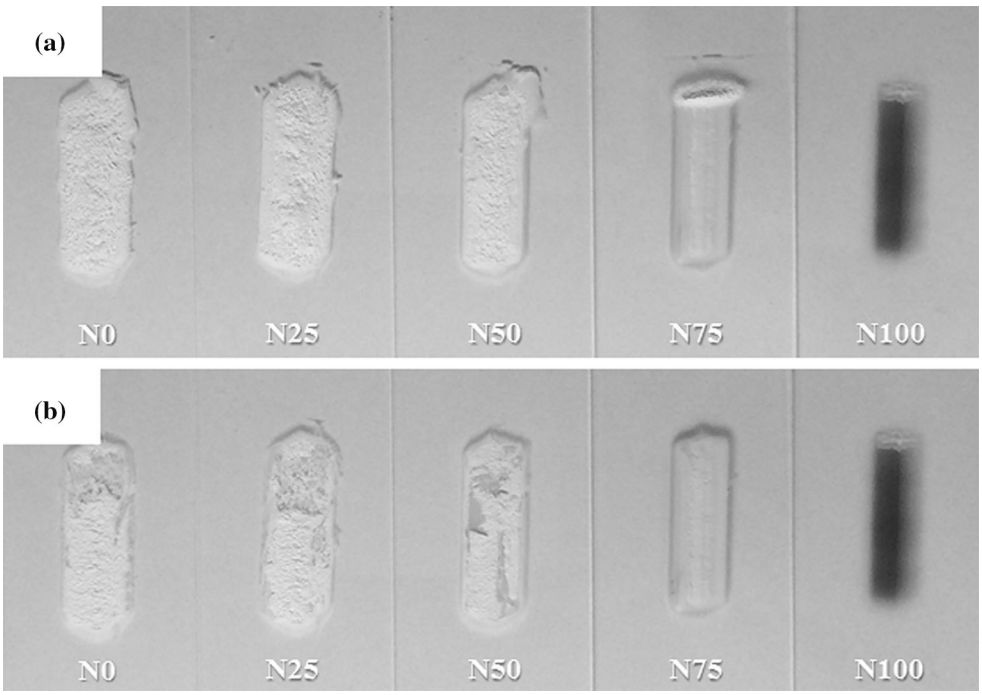

Fig. 4 Film shapes of each blended powder (a) before and (b) after ultrasonication

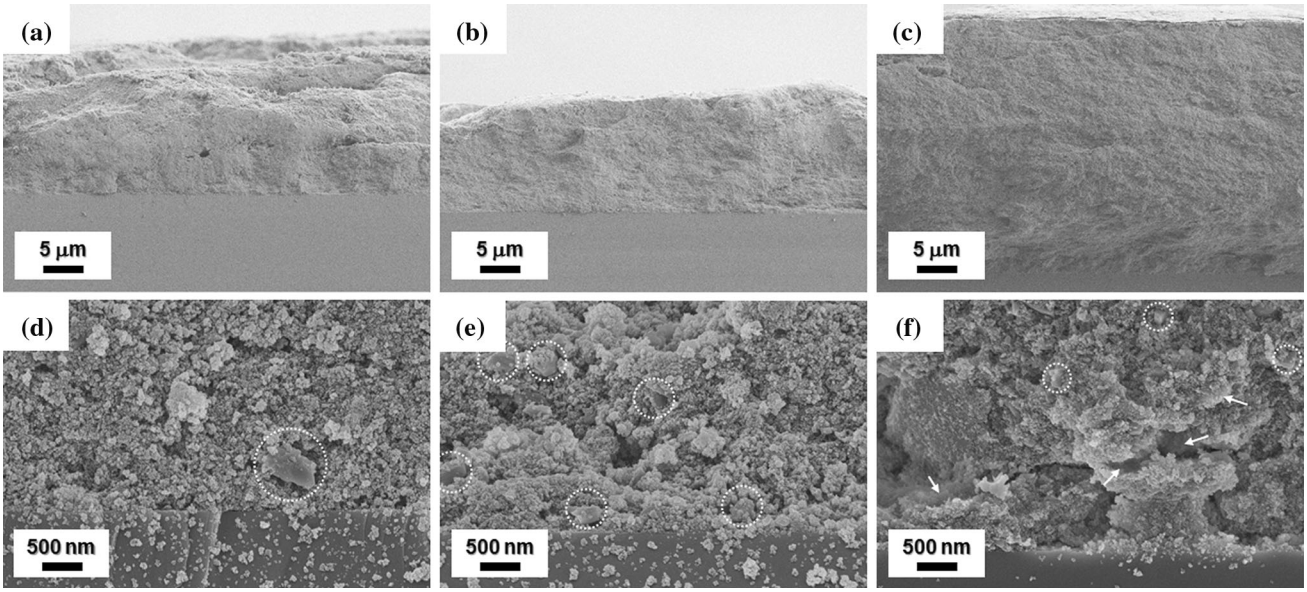

Fig. 5 FE-SEM cross-sectional micrographs of the deposited forms fabricated using (a, d) N25, (b, e) N50, and (c, f) N75 blended powders [(a)-(c) low-magnification images and (d)-(f) higher-magnification images of regions in (a)-(c), respectively]

notice. First, relatively large fragments were more frequently found in the layer with a high fraction of nano-Al_2O_3, as marked by the white dashed circles, while the size decreased as the amount of submicron powder increased. As a result, it can be speculated that particle fragmentation occurred more severely as the fraction of submicron Al_2O_3 increased. Considering that nano- and submicron particles impacted on the substrate with similar impact velocities, it is thought that nanoparticles suppressed the fragmentation of submicron particles as soft material in a composite coating of ceramic and polymer did (Ref 18). In a previous research, Park et al. mentioned that nanoparticles were not easily fragmented due to their high surface energy, and instead, they underwent elastic/plastic deformation. In addition, some of the kinetic energy was consumed to break the inter-particle bonding among nanoparticles in an agglomerated form, rather than particle fragmentation (Ref 5, 9). In other words, in blended powders, nanoparticles play a role of shock absorption in place of submicron particles, which helps to preserve the submicron Al_2O_3 from fragmentation. Second, evidence of densification was observed in the layer fabricated using N75 powder, as marked by the white arrows in Fig. 5(f). It is believed that this evidence was generated by severe friction among the deposited particles. Considering that the densified surface was usually found when using a relatively high fraction of submicron particles, it seems that the densification was attributed to severe friction which results from the high-velocity impact of large particles. As a result, it is hypothesized that large particles contribute to consolidation via friction-induced densification at the interfaces. In this respect, the tendency of bonding strengthening depending on the fraction of each particle size is in good agreement with the results of detachment after ultrasonication shown in Fig. 4.

Figure 6 shows the top view of each deposited form in Fig. 5. As shown in Fig. 6(a)-(c), the surface became roughened as the fraction of nanoparticles increased, which is in good agreement with the particle size effect observed in a previous study (Ref 5). In addition, it was clearly observed that larger fragments were observed on the surface more frequently as the amount of small particles increased, as confirmed in Fig. 6(d)-(f). Considering the fact that the fragments remained on the surface after ultrasonication, it seems that the fragments were slightly attached there despite weak bonding. However, it is thought that as the impact of large particles is frequent, the large fragments undergo further fragmentation, and simultaneously, the friction occurring among particles becomes severe, leading to densification such as the tamping effect. Therefore, even though the content of large particles increased, the surface became rather smooth. In this regard, it is anticipated that the film microstructure and bonding strength can be controlled by adjusting ratio of the two powders with different particle sizes.

Thick Film Formation and Densification

Figure 7 shows the cross-sectional FE-SEM micrographs of the thick Al_2O_3 films fabricated using the N90, N95, and N100 powders. Figure 7(d)-(f) shows higher-magnification images of Fig. 7(a)-(c). Similar with the first trial, the

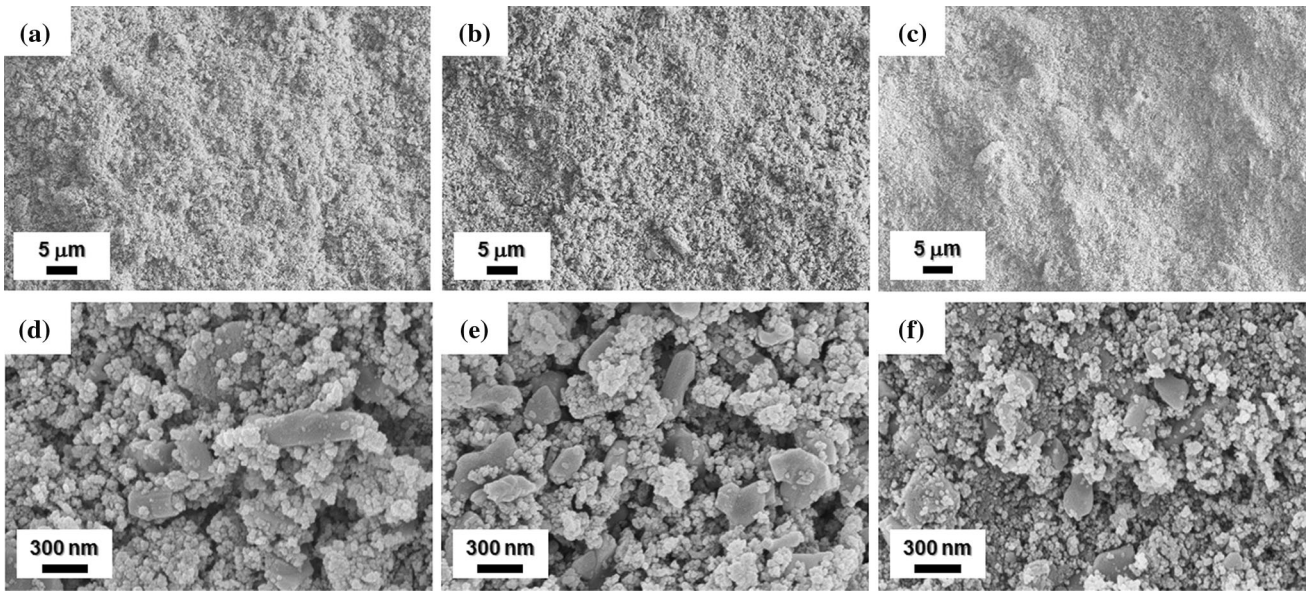

Fig. 6 FE-SEM micrographs of the morphology of the deposited forms fabricated using (a, d) N25, (b, e) N50, and (c, f) N75 blended powders [(a)-(c) low-magnification images and (d)-(f) higher-magnification images of regions in (a)-(c), respectively]

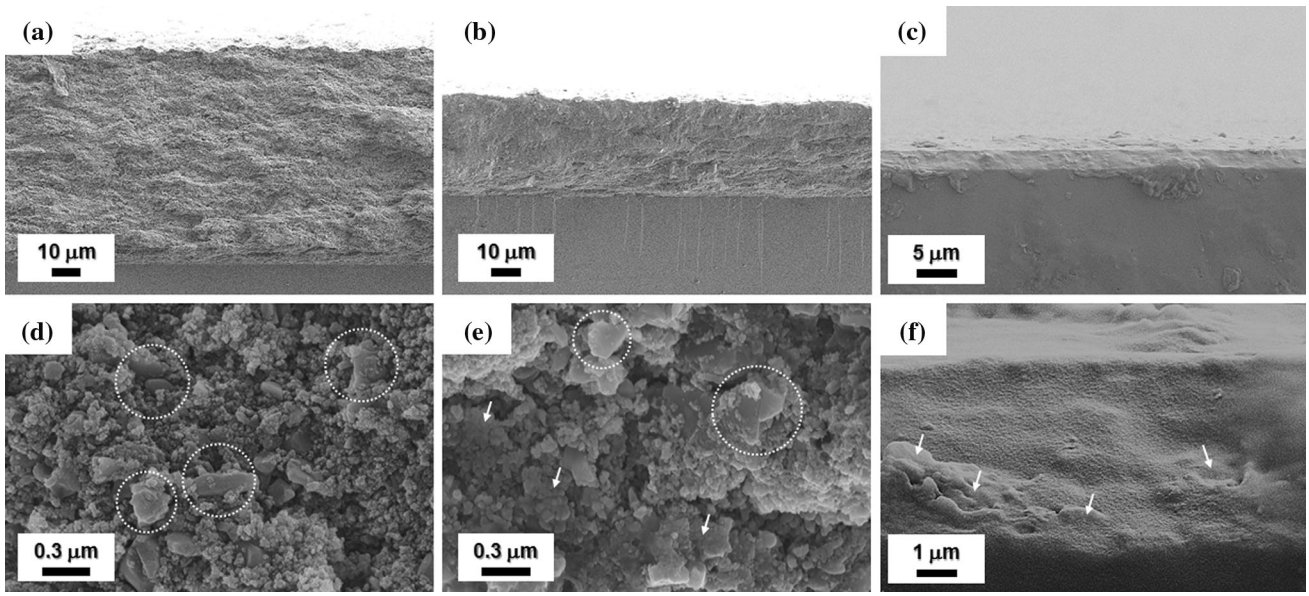

Fig. 7 FE-SEM cross-sectional micrographs of thick Al_2O_3 films fabricated using the (a, d) N90, (b, e) N95, and (c, f) N100 powders [(a)-(c) low-magnification images and (d)-(f) higher-magnification images of regions in (a)-(c), respectively]

cross-sectional microstructures were changed as the ratio of Al_2O_3 powder was varied. When the amount of nano-Al_2O_3 was relatively higher (N90), intact submicron particles were clearly observed and the boundaries between particles were obvious. In case of N95 coating, although some submicron particles were still intact, deformed submicron particles were greatly increased and boundaries between nanoparticles became faint. As only submicron Al_2O_3 was used, the crystallites and its boundaries were undistinguishable. Some flattened particles and traces shows that the relatively dense coating was deposited by strong impulse.

The thickness significantly increased from around 2.3 to 69.9 μm as the fraction of nano-Al_2O_3 increased from 0 to 10%, as shown in Fig. 8. The deposition rates were determined to be 0.688 μm/min (N100), 7.087 μm/min (N95), and 20.979 μm/min (N90). The increase in the deposition rate in this research is notable because, in

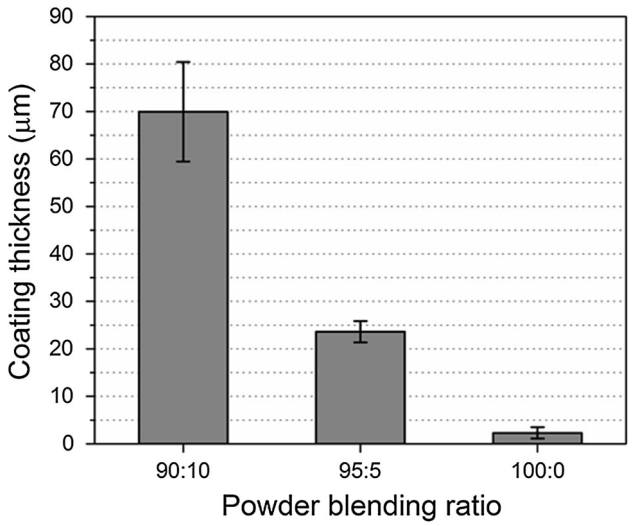

Fig. 8 Coating thicknesses with different blending ratios

general, it is in the range of 1-3 μm/min (Ref 1, 2). Additionally, the deposition efficiencies were roughly estimated to 0.126% (N100), 1.064% (N95), and 2.154% (N90). The efficiency of the N90 powder is very meaningful because as far as we know, the deposition efficiency in the VKS process has been limited to around 0.1% and it has been widely accepted that is difficult to surpass 1% (Ref 4). The reason for great increment of the coating thickness is still unclear; however, it is obvious that nano-Al_2O_3 particles are easily attached and stayed on the surface of the substrate or pre-deposited layer. It is carefully expected that the high surface energy of nanoparticles induced the bonding. But, this bonding is so weak that the mechanical properties of film are poor (it will be discussed later in this paper). The coating density was measured to 3.74 g/cm^3 (N100), 3.03 g/cm^3 (N95), and 2.01 g/cm^3 (N90). When the density of fully dense Al_2O_3 was 3.95 g/cm^3, as the amount of nano-Al_2O_3 addition increased, the density of coating was decreased up to 51% of its bulk density. Consequently, it can be concluded that the deposition rate and efficiency can be controlled by the combination of different particle sizes and the coating density can be changed.

Figure 9 shows the film morphologies fabricated using N90, N95, and N100. In Fig. 9(a)-(c), it can be confirmed that the surface became significantly smoothened in comparison with the morphologies of N25, N50, and N75 shown in Fig. 6. Although not completely fragmented parts were still observed, it seems that most particles were fragmented well at the other regions consisting of nanocrystalline fragments. Another interesting point is the evidence of plasticity. In Fig. 9(e)-(f), a flattened surface appeared and the interface between fragments became blurred as the interfaces were indistinguishable. As mentioned above, this is attributed to the friction-induced densification generated by the impact of large particles. Because of this, the previously deposited fragments underwent fragmentation with plasticity (Ref 7). Moreover, considering that it is possible for nanoceramic particles to be plastically deformed, after a particle is sufficiently fragmented, the generated nanofragments consume the excessive kinetic energy by plastic deformation (Ref 19).

Figure 10 displays various evidences of the consolidation phenomena through which the consolidation process can be presumed. In Fig. 10(a), a large crater was observed (N25), which may be generated via a process in which a large particle is impacted with high velocity and it is stuck in the weakly deposited nano-Al_2O_3 (shock absorption effect), as marked by the pale red arrow. Then, it falls out leaving the crater without sufficient bonding. When the fraction of sub-Al_2O_3 increased (N75), the dent evidence was remarkable. It is clearly observed that the fragments underneath the craters were tamped at the dent region, as marked by yellow arrows in Fig. 10(b). After sub-particles were sufficiently used, the fragmentation became distinct and the surface was severely tamped, as the original particle is indistinguishable in Fig. 10(c). In the figure, it appears that nano-Al_2O_3 stayed just on the surface without strong bonding. When using 100% sub-Al_2O_3 particles, a smooth surface with indistinguishable interfaces was formed by sufficient friction, as shown in Fig. 10(d). Thereby, a dense microstructure with a smooth surface, a typical VKS film shape, is achieved (Ref 2, 9, 15).

Film Mechanical Properties and Bonding Consolidation

As confirmed in Fig. 4, the pressed compact form was easily detached even by ultrasonication, but when exceeding a 75% ratio of submicron Al_2O_3, it can endure weak external stress (N75 in Fig. 4). This is important for applying ceramic films or patterns in industrial fields. Figure 11(a) represents the change of adhesive strength depending on the powder blending ratio. Clearly, as the fraction of submicron Al_2O_3 increased from 90 to 100%, the adhesive strength of the film increased from 12.89 N to 26.68 N. In the case of adhesion, the anchoring layer effect needs to be considered. In VKS, an anchoring layer plays an important role for film adhesion (Ref 2, 20). The layer formation is generally related to the initial particle impact at the beginning of deposition with surface erosion of the substrate. In addition, the anchoring layer is affected by the impact velocity and the impulse (substrate gained) as well as the material combination between the powder and substrate (Ref 5, 21, 22). In this study, assuming that the used substrate material and the impact velocity were the same, the anchoring layer formation and its effect were

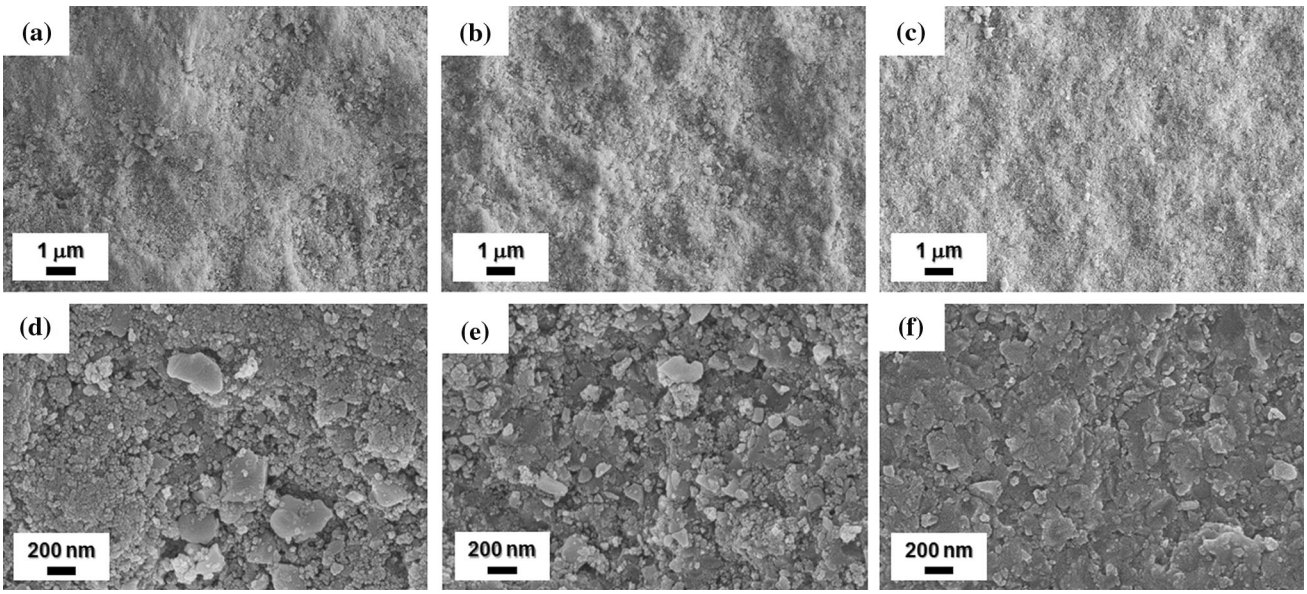

Fig. 9 FE-SEM micrographs of the morphology of the films fabricated using (a, d) N90, (b, e) N95, and (c, f) N100 blended powders [(a)-(c) low-magnification images and (d)-(f) higher-magnification images of regions in (a)-(c), respectively]

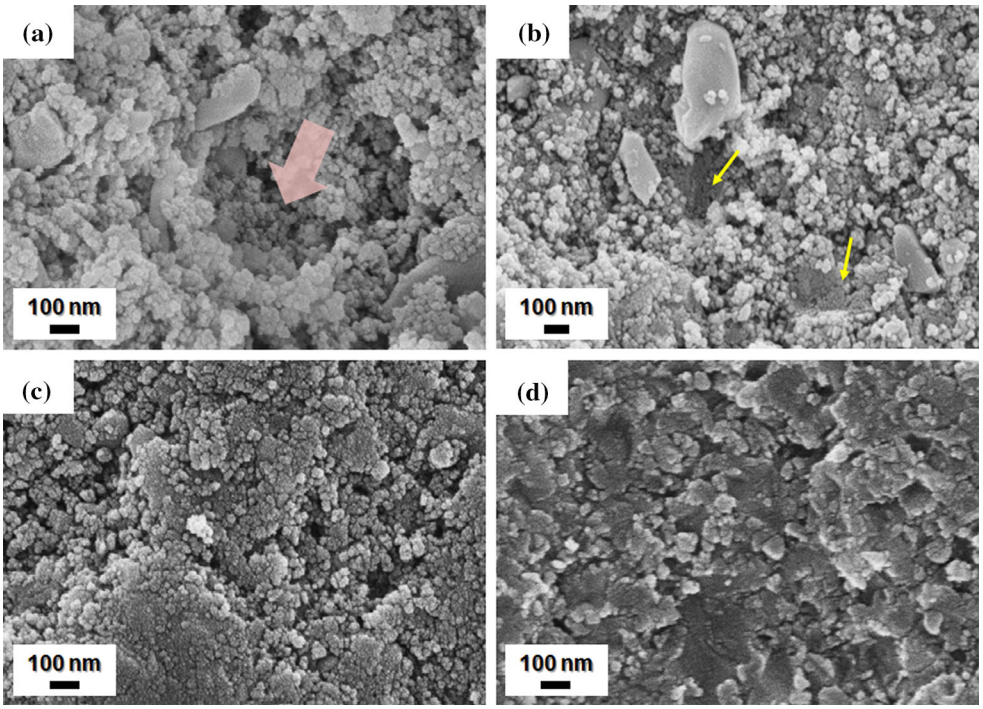

Fig. 10 FE-SEM micrographs of the evidences of the consolidation phenomena: (a) crater (N25), (b) consolidation (N75), (c) insufficient consolidated surface (N90), and (d) dense morphology resulting from sufficient impact-induced consolidation (N100)

determined by the impulse caused by the initial particle state, which is either a dense and bulk shape (submicron Al_2O_3) or a porous and agglomerated shape (nano-Al_2O_3). Depending on the powder state, the impulse that the substrate gained was different, in spite of a similar impact velocity (Ref 5). Consequently, as the fraction of sub-particles increased, the impulse increased, by which the adhesive strength was improved.

In addition to adhesion, the cohesive bonding strength (among fragments) is also an important factor to prevent film delamination within the coating layer. Figure 11(b) demonstrates the nanohardness and elastic

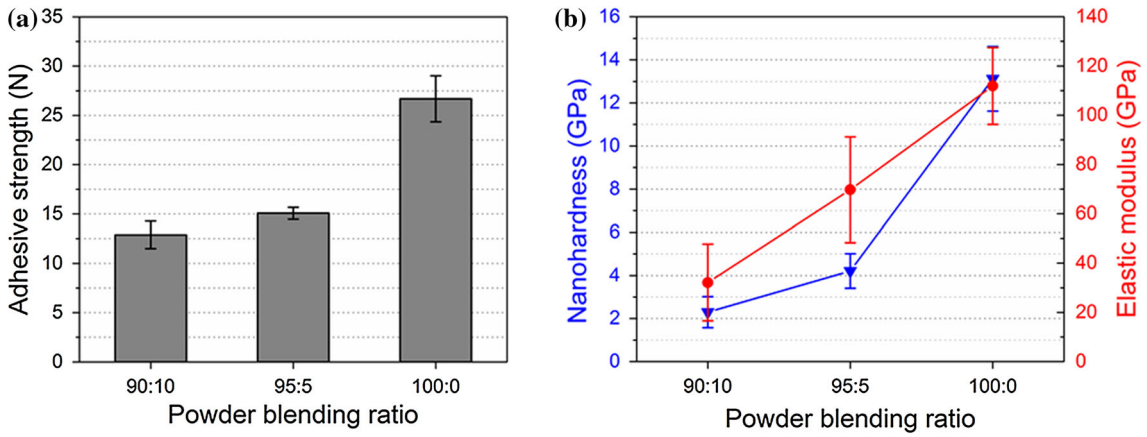

Fig. 11 The (a) adhesive strength and (b) nanohardness and elastic modulus of the films fabricated using N90, N95, and N100 powders

modulus of the films fabricated using N90, N95, and N100. It was obviously confirmed that the nanohardness and elastic modulus gradually decreased from 13.12 to 2.3 GPa and from 111.89 to 32.14 GPa, respectively, as the ratio of nano-Al_2O_3 was increased from 0% (N100) to 10% (N90). Although, in general, the elastic modulus represents the atomic bonding strength, it is thought that the low elastic modulus indicates weakened bonding among fragments because the strength among fragments was estimated to be lower than among atoms. Moreover, even though films fabricated by the VKS process usually show slightly deteriorated properties because they consist of a nanocrystalline phase and shock-induced damage, the densification process is essential to strengthen the bonding among fragments (Ref 7, 8). Overall, mechanical properties of Al_2O_3 coatings were degraded as the addition of nano-Al_2O_3 increased. This can be proved through the calculated density, microstructure of coating as mentioned above. Due to nanoparticles, a coating with more open structure was formed, and the bonds between crystallite and the coating–substrate were weakened. These results correspond well with the result of L. Wang et al. They also fabricated the Al_2O_3 film with different particle sizes using vacuum cold spraying (VCS) which is almost similar process with VKS. As already mentioned in Introduction, the nano- and submicron-sized Al_2O_3 particles were selected as feedstock materials. The nanohardness data showed that the submicron Al_2O_3 film had an around 7.8 Gpa; however, the nano-Al_2O_3 film only reached an average of 3.5 GPa. The authors also stated that the nanoparticles with agglomerated form could absorb some part of the impact energy (Ref 13). Thus, it can be proposed that the mechanical properties of the VKS coating are closely related to the density of the coating. Usually, as the film density increases, the hardness of film increases.

The Role of the Particle Size in the Deposition Process

Based on the evidence obtained from the analysis of the microstructure and mechanical properties, the role of particles with different sizes in VKS deposition is discussed in this section. Figure 12(a)-(i) schematically shows the deposition behaviors depending on the use of only (a)-(c) nano-, (d)-(f) submicron, and (g)-(i) blended particles. In the case of only using nanoparticles, the particles were severely agglomerated with each other (Fig. 12a), and thus, when impacting onto the substrate, a considerable portion of the impact energy (impulse) is spent breaking the agglomerated form into primary particles (Fig. 12b). In other words, the agglomerated form creates an effect of shock absorption itself at the time of impact. In addition, since primary nanoparticles have a very high surface energy, they are not further fragmented and just consume the remaining energy in elastic/plastic deformation (hardly fragmentation). Therefore, the bonding among nanoparticles is achieved by only a low friction energy at the interfaces of the particles without new (activated) surface energy occurring during fragmentation (Fig. 12b). We believe that the low cohesive bonding can be ascribed to the lack of surface energy with low friction energy. Moreover, the impulse that the substrate gains is also low because of the energy consumed in particle breaking. Thus, the anchoring layer is not properly formed, which makes the adhesion low. As a result, the nanoparticles can be directly deposited without additional fragmentation, by which the probability of particle loss (no participation for deposition) decreases and the deposition efficiency increases. In contrast, a porous coating layer is formed due to inadequate bonding energy resulting from the low activated surface energy and/or friction energy, leading to a low bonding strength (Fig. 12c).

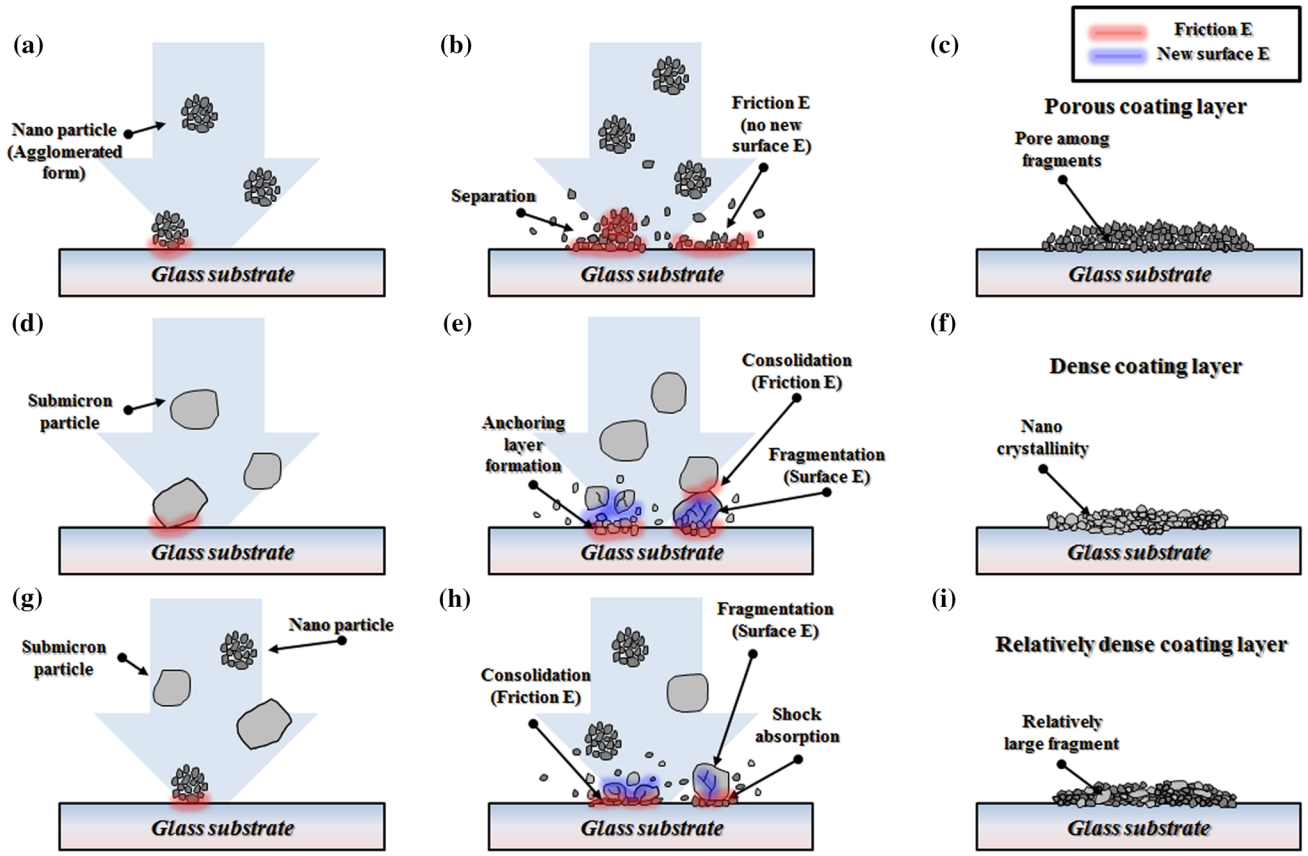

Fig. 12 Schematic illustration of the particle deposition process using (a)-(c) only nanosized particles, (d)-(f) submicron-sized particles, and (g)-(i) blended particles

On the other hand, the case of only using sub-particles is significantly different from that of nanoparticles, as shown in Fig. 12(d)-(f). The particles cannot be directly deposited themselves. At the initial stage of particle impact, the particle undergoes dynamic fragmentation alongside shock-induced plasticity (Ref 7, 8), during which a high interfacial friction energy and activated surface energy occur (Fig. 12e). This process is repeated by subsequent particle impacts. Thus, the energy transferred to bonding is accumulated as deposition proceeds. In this deposition mechanism, the particle is not deposited itself, but the small fragments after sufficient fragmentation are deposited (indirect deposition). From previous researches, the size of fragments in the coating layer is usually in the range of 5-20 nm (Ref 1, 2). In this respect, we conclude that for strong bonding in VKS, the size of fragments should be sufficiently small with sizes of up to several or several tens of nanometers. Thereby, a high activated surface energy and interfacial friction energy by fragment plasticity occur and are transformed to bonding energy. Nanosized fragments can be plastically deformed, such as nanospheres (Ref 19), by which interfacial friction is generated. That is, the nanosized fragment is not the output of the deposition process, but a prerequisite for strong bonding among fragments in VKS. Furthermore, the impulse to the substrate is high compared to nanoparticles and the friction between the substrate and particle is severe considering the dynamic fragmentation process. Therefore, an anchoring layer is formed with sufficiently strong adhesion. Consequently, a strong bonding strength is achieved by the anchoring layer (adhesion) and dense microstructure (cohesion) (Fig. 12f), by which the mechanical properties are improved. However, it is considered that the probability of generated fragment loss is very high in this indirect deposition, and thus, the deposition efficiency is deteriorated.

When blended powder is used, nano- and submicron particles play different roles in deposition, as shown in Fig. 12(g)-(i). At the beginning of deposition, nanoparticles are directly deposited via breaking the bonding among primary particles. Although they weakly adhere on the surface, a large portion of them take part in deposition. Then, submicron particles impact onto the deposited nanoparticle stack and the interfacial bonding among nanoparticles is consolidated by severe friction occurring from the high impulse of submicron particles (tamping effect) (Fig. 12h). Furthermore, deposited nanoparticles

absorb the shock energy generated by the impact of the sub-particle and suppress fragmentation of submicron particles (shock absorption effect) (Fig. 12h). That is, nanoparticles contribute to a high deposition rate and efficiency, where they are first deposited by themselves with a relatively low loss of particles. Secondly, they help to preserve sub-particles from fragmentation, which decreases the loss of fragments of submicron particles. On the other hand, submicron particles play roles of anchoring layer formation and bonding consolidation. Thus, the deposition behaviors and mechanical properties can be controlled using the respective characteristics of nano- and submicron particles.

Based on the results obtained herein, it is believed that the particles in a powder play different roles depending on their size. In general, one kind of powder is usually used in VKS. In addition, a manufactured powder usually has a certain particle size distribution. Due to technical difficulties to precisely separate particles based on their size, a powder has an average submicron size in reality, and therefore, it is important to control the size distribution to achieve a proper deposition rate (or efficiency) with properties for application. In addition, a bimodal powder can also be a good candidate to improve the deposition rate (or efficiency). Although further optimization is needed to maximize the film properties, the findings in this research are very crucial to overcome the problem of a low deposition efficiency and widen its application to various fields, including thick ceramic films, three-dimensional printing, and ceramic bulk fabrication.

Conclusion

In this study, the role of particles with different sizes in vacuum kinetic spraying was investigated using different blended powders with various ratios. Due to the small size of nano-Al_2O_3, the particles could be deposited directly without additional fragmentation, thereby greatly increasing the deposition rate and efficiency of the system. On the other hand, submicron Al_2O_3 induced an intense impulse on the substrate and particles, resulting in anchoring layer formation and densification of the coating. This enhanced the cohesion and adhesion of the coating system. Thus, it was demonstrated that nanoparticles were mainly involved in deposition phenomena which build up the coating and submicron particles contribute to anchoring layer formation and consolidation during the process. Because the VKS coating is fabricated by complex phenomenon of the bimodal state powder, it is emphasized that the proper distribution of the feedstock powder is critical in determining the film microstructure and properties.

Acknowledgment This work was supported by World Class 300 Project R&D Support project (www.worldclass300.or.kr) funded by the Small and Medium Business Administration (SMBA, Korea) [Project Name:Development of Plasma-resistant Surface Treatment Technology for 3D-structure and Large-area Parts of Semiconductor/Display Fabrication Equipments].

References

1. J. Akedo, Aerosol Deposition of Ceramic Thick Films at Room Temperature: Densification Mechanism of Ceramic Layers, *J. Am. Ceram. Soc.*, 2006, **89**(6), p 1834-1839
2. J. Akedo, Room Temperature Impact Consolidation (RTIC) of Fine Ceramic Powder by Aerosol Deposition Method and Application to Microdevices, *J. Therm. Spray Technol.*, 2008, **17**(2), p 181-198
3. D. Hanft, J. Exner, M. Schubert, T. Stocker, P. Fuierer, and R. Moos, An Overview of the Aerosol Deposition Method: Process Fundamentals and New Trends in Materials Applications, *J. Ceram. Sci. Technol.*, 2015, **6**(3), p 147-182
4. K. Naoe, M. Nishiki, and A. Yumoto, Relationship Between Impact Velocity of Al_2O_3 Particles and Deposition Efficiency in Aerosol Deposition Method, *J. Therm. Spray Technol.*, 2013, **22**(8), p 1267-1274
5. H. Park, H. Kwon, and C. Lee, Inflight Particle Behavior in the Vacuum Kinetic Spray Process, *J. Therm. Spray Technol.*, 2017, **26**(7), p 1616-1631
6. M. Lebedev, J. Akedo, K. Mori, and T. Eiju, Simple Self-Selective Method of Velocity Measurement for Particles in Impact-Based Deposition, *J. Vac. Sci. Technol., A*, 2000, **18**(2), p 563-566
7. H. Park, J. Kwon, I. Lee, and C. Lee, Shock-Induced Plasticity and Fragmentation Phenomena During Alumina Deposition in the Vacuum Kinetic Spraying Process, *Scripta Mater.*, 2015, **100**, p 44-47
8. H. Park, J. Kim, and C. Lee, Dynamic Fragmentation Process and Fragment Microstructure Evolution of Alumina Particles in a Vacuum Kinetic Spraying System, *Scripta Mater.*, 2015, **108**, p 72-75
9. H. Park, J. Kim, S. Lee, and C. Lee, Correlation of Fracture Mode Transition of Ceramic Particle with Critical Velocity for Successful Deposition in Vacuum Kinetic Spraying Process, *J. Therm. Spray Technol.*, 2017, **26**(3), p 327-339
10. D. Lee, H. Kim, and S. Nam, Effects of Starting Powder on the Growth of Al_2O_3 Films on Cu Substrates Using the Aerosol Deposition Method, *J. Korean Phys. Soc.*, 2010, **57**(4), p 1115-1121
11. D. Lee, H. Kim, Y. Kim, Y. Yun, and S. Nam, Growth Process of α-Al2O3 Ceramic Films on Metal Substrates Fabricated at Room Temperature by Aerosol Deposition, *J. Am. Ceram. Soc.*, 2011, **94**(9), p 3131-3138
12. J. Exner, M. Hahn, M. Schubert, D. Hanft, P. Fuierer, and R. Moos, Powder Requirements for Aerosol Deposition of Alumina Films, *Adv. Powder Technol.*, 2015, **26**, p 1143-1151
13. L. Wang, H. Zhou, K. Zhang, Y. Wang, C. Li, X. Luo, G. Yang, and C. Li, Effect of the Powder Particle Structure and Substrate Hardness During Vacuum Cold Spraying of Al_2O_3, *Ceram. Int.*, 2017, **43**, p 4390-4398
14. A. C-05, Standard Test Method for Adhesion Strength and Mechanical Failure Modes of Ceramic Coatings by Quantitative Single Point Scratch Testing, 2005
15. F. Cao, H. Park, J. Heo, J. Kwon, and C. Lee, Effect of Process Gas Flow on the Coating Microstructure and Mechanical

Properties of Vacuum Kinetic-Sprayed TiN Layers, *J. Therm. Spray Technol.*, 2013, **22**(7), p 1109-1119
16. J. Kwon, H. Park, I. Lee, and C. Lee, Effect of Gas Flow Rate on Deposition Behavior of Fe-Based Amorphous Alloys in Vacuum Kinetic Spray Process, *Surf. Coat. Technol.*, 2014, **259**, p 585-593
17. J. Kim, H. Kwon, H. Park, and C. Lee, Microstructural Features Affecting Optical Properties of Vacuum Kinetic Sprayed Al_2O_3 Thin Film, *Surfaces and Interfaces*, 2017, **9**, p 114-123
18. H. Kim and S. Nam, High Loading of Nanostructured Ceramics in Polymer Composite Thick Films by Aerosol Deposition, *Nanoscale Res. Lett.*, 2012, **7**(1), p 92
19. E. Calvie, L. Joly-Pottuz, C. Esnouf, P. Clement, V. Garnier, J. Chevalier, Y. Jorand, A. Malchere, T. Epicier, and K. Masenelli-Varlot, Real Time TEM Observation of Alumina Ceramic Nano-Particles During Compression, *J. Eur. Ceram. Soc.*, 2012, **32**(1), p 2067-2071
20. Y. Kim, J. Lee, H. Kim, Y. Yun, and S. Nam, Silver Metallization for Microwave Device Using Aerosol Deposition, *Ceram. Int.*, 2012, **38**, p S201-S204
21. D. Lee, H. Kim, Y. Kim, M. Jeon, and S. Nam, Substrate Hardness Dependency on Properties of Al_2O_3 Thick Films Grown by Aerosol Deposition, *Surf. Coat. Technol.*, 2012, **209**, p 160-168
22. J. Kim, J. Lee, D. Park, and E. Park, Enhancement of Interface Anchoring and Densification of Y_2O_3 Coating by Metal Substrate Manipulation in Aerosol Deposition Process, *J. Appl. Phys.*, 2015, **117**(1), p 014903